Journal of Pharmaceutical and Biomedical Analysis 240 (2024) 115966

Contents lists available at ScienceDirect

Journal of Pharmaceutical and Biomedical Analysis

journal homepage: www.journals.elsevier.com/journal-of-pharmaceutical-and-biomedical-analysis

Untargeted metabolomics of bladder tissue using liquid chromatography and quadrupole time-of-flight mass spectrometry for cancer biomarker detection

Joanna Nizioł [a,*], Krzysztof Ossoliński [b], Aneta Płaza-Altamer [a], Artur Kołodziej [a], Anna Ossolińska [b], Tadeusz Ossoliński [b], Zuzanna Krupa [c], Tomasz Ruman [a]

[a] Rzeszów University of Technology, Faculty of Chemistry, 6 Powstańców Warszawy Ave., 35-959 Rzeszów, Poland
[b] Department of Urology, John Paul II Hospital, Grunwaldzka 4 St., 36-100 Kolbuszowa, Poland
[c] Doctoral School of Engineering and Technical Sciences at the Rzeszów University of Technology, 8 Powstańców Warszawy Ave., 35-959 Rzeszów, Poland

ARTICLE INFO

Keywords:
Bladder cancer
Biomarkers
Human tissue
Metabolomics
LC-MS
UHPLC-UHRMS

ABSTRACT

Bladder cancer (BC) ranks among the most common cancers globally, with an increasing occurrence, particularly in developed nations. Utilizing tissue metabolomics presents a promising strategy for identifying potential biomarkers for cancer detection. In this study, we utilized ultra-high-performance liquid chromatography coupled with ultra-high-resolution mass spectrometry (UHPLC-UHRMS), incorporating both C18-silica and HILIC columns, to comprehensively analyze both polar and non-polar metabolite profiles in tissue samples from 99 patients with bladder cancer. By utilizing an untargeted approach with external validation, we identified twenty-five tissue metabolites that hold promise as potential indicators of BC. Furthermore, twenty-five characteristic tissue metabolites that exhibit discriminatory potential across bladder cancer tumor grades, as well as thirty-nine metabolites that display correlations with tumor stages were presented. Receiver operating characteristics analysis demonstrated high predictive power for all types of metabolomics data, with area under the curve (AUC) values exceeding 0.966. Notably, this study represents the first report in which human bladder normal tissues adjacent to cancerous tissues were analyzed using UHPLC-UHRMS. These findings suggest that the metabolite markers identified in this investigation could serve as valuable tools for the detection and monitoring of bladder cancer stages and grades.

1. Introduction

Bladder cancer (BC), also known as urological or urinary bladder cancer, ranks as the tenth most common and thirteenth most deadly cancer worldwide. According to the latest GLOBOCAN data, bladder cancer represents around 3% of all cancer cases globally. Its occurrence is on the rise, especially in developed countries, with approximately 550,000 new cases being diagnosed each year [1]. Environmental and occupational factors play a significant role in the development of bladder cancer, with tobacco smoke being the most significant risk factor, responsible for nearly 50% of bladder tumors. Smokers face a 2.5-fold higher risk compared to nonsmokers. Approximately 7% of bladder cancer cases are attributed to hereditary genetic predisposition [2].

BC is a diverse condition with a significant risk of morbidity and recurrence. BC manifests in both primary and recurrent forms, with stages ranging from T1 to T4, including Ta [3]. Currently, BC diagnosis primarily relies on urinary cytology, cystoscopy, and radiological imaging. Cystoscopy, though, is invasive, painful, expensive, and less effective in detecting high-grade superficial tumors, often causing considerable psychological stress, especially when combined with a biopsy. Urinary cytology, while noninvasive and highly specific, lacks sensitivity [4].

Recent advancements in BC research have led to the development of several biomarkers primarily based on protein detection. However, none of these biomarkers have been incorporated into clinical practice guidelines due to their insufficient diagnostic performance at the time of evaluation, high identification costs, and the need for sophisticated instrumentation, which is not commonly accessible to many clinicians. Consequently, there are currently no clinically viable biomarkers for the

* Corresponding author.
E-mail address: jniziol@prz.edu.pl (J. Nizioł).

https://doi.org/10.1016/j.jpba.2024.115966
Received 27 September 2023; Received in revised form 18 December 2023; Accepted 4 January 2024
Available online 8 January 2024

early detection, diagnosis, or prognosis of BC [5].

Metabolomics stands out as a potent method for detecting low molecular compounds in biological samples, playing a crucial role in understanding disease processes [6]. It focuses on the changes in metabolites, which are often the result of disruptions in biochemical pathways caused by diseases. These alterations in metabolites have gained increasing recognition as vital indicators in clinical diagnostics. As a result, metabolomics has become a leading technique in the identification of biomarkers, early disease detection, and the exploration of related biochemical pathways. By analyzing metabolites present in biological samples such as urine, serum, and tissue, metabolomics enables the monitoring of the metabolic response of living systems to diseases or drug toxicity. A key advantage of metabolomics is its capacity to simultaneously detect hundreds of metabolites, offering a comprehensive view of biochemical changes [7].

In the past two decades, two main analytical platforms, mass spectrometry (MS) and nuclear magnetic resonance spectroscopy (NMR), have been predominantly utilized for metabolomic analysis of various bladder cancer samples [8]. Each of these techniques has its advantages and disadvantages. NMR stands out for its minimal preparation requirements, speed, non-destructive nature, and highly consistent results. Its advantages also include the ability to analyze a wide array of sample types such as liquid, gas, solid, and tissue, enhancing its versatility. However, NMR faces limitations in sensitivity, posing a challenge for future advancements in this area. NMR often requires a larger amount of sample compared to other techniques like MS, which can be a limitation when sample availability is restricted. Moreover, for samples with a large number of different metabolites, the spectral resolution of NMR might not be sufficient to distinguish between closely related compounds. In contrast, MS demonstrates superior specificity and sensitivity, making it a more effective technique. MS can analyze a wider range of compounds, including those that are non-volatile or thermally unstable, which NMR might not effectively analyze. MS generally requires a smaller amount of sample for analysis compared to NMR, which is advantageous when sample availability is limited. MS is generally less affected by the complexity of the sample matrix, which can be a challenge in NMR analysis. While both NMR and MS can be used for quantitative analysis, MS is often preferred for its ability to handle complex mixtures and provide highly accurate quantitative data. Moreover, MS can be coupled with various separation techniques like Liquid Chromatography (LC) or Gas Chromatography (GC), enhancing its ability to analyze complex mixtures by separating compounds before detection [9].

The data derived from NMR and MS experiments in metabolomics are often intricate, offering both qualitative and quantitative insights into numerous metabolites. Metabolomics data, known for their high variability and susceptibility to noise, are influenced by factors like environment, diet, age, lifestyle, medications, microbiota, and sample handling. They also exhibit a higher degree of missing data, complicating multivariate analysis and classification. Therefore, it's crucial to apply suitable statistical methods to avoid losing important information or identifying incorrect trends and models. In metabolomics, multivariate statistical analysis is preferred for its comprehensive approach to studying system-level changes in biological systems. This analysis includes both unsupervised methods like Principal Component Analysis (PCA), mainly used for quality control, and supervised methods like Partial Least Square Discriminant Analysis (PLS-DA) and its advanced form, Orthogonal PLS-DA (OPLS-DA), which are crucial for biomarker discovery. These techniques help in effectively breaking down and analyzing predictor variables, with OPLS-DA providing clearer models by distinguishing predictive variance from noise [10].

However, the literature on human bladder tissue analysis in the context of metabolomics remains limited. The initial exploration of metabolomic profiling in bladder tissues was conducted in 2011 by Putluri et al. using LC-MS. Their analysis of 58 tissues unveiled significant alterations in the levels of 35 mass spectral features within the bladder tissues [11]. In 2013, Tripathi et al. employed the high-resolution magic angle spinning (MAS) NMR technique to conduct further research. They identified 22 distinct metabolites associated with different stages of bladder cancer. These findings were cross-validated using targeted GC-MS analysis, although normal, unaffected tissues were not included as controls [12]. Another study, published in 2017 by Piyarathna et al., examined 165 bladder tissues, comprising 126 bladder cancer tissues and 39 benign or normal adjacent tissues. Through UHPLC-HRMS analysis, they discovered 570 lipids associated with the survival and diverse clinical stages of bladder cancer [13]. In addition, our recent study employed nanoparticle-based laser desorption/ionization mass spectrometry imaging (LDI-MSI) to investigate BC tissues. This innovative approach allowed us to identify 10 potential biomarkers associated with this disease by analyzing the distinct distribution patterns of these compounds on the surface of the imaged tissue fragment [14].

To discern specific cellular markers that can differentiate between different grades and stages of BC, numerous metabolomics studies have been conducted on urine and blood samples from BC patients [7]. However, to the best of our knowledge, only a few studies have examined the associations between alterations in metabolite levels in tissues from BC patients and the specific grades and/or stages of tumor progression [4,12,15].

The identification of BC tissue biomarkers could potentially be crucial for understanding cancer mechanisms at a molecular level and aiding in the development of targeted therapies. These biomarkers might be more specific to certain cancer types than blood biomarkers and could be invaluable in identifying bladder cancer subtypes for personalized treatment and prognosis. They might also be essential in monitoring treatment responses and detecting recurrences, offering insights not always available from serum biomarkers [16]. In the context of surgical interventions, particularly in procedures like transurethral resection of bladder tumor (TURBT) or partial cystectomy, BC tissue biomarkers could play a significant role. Surgeons might aim to remove the tumor while conserving as much healthy tissue as possible, but visually differentiating between cancerous and normal tissue can be challenging, especially with small tumors or unclear margins. Biomarkers specific to bladder cancer could provide molecular information that might help identify tumor boundaries, potentially enhancing the precision of these surgeries. Furthermore, tissue biomarkers could potentially be used during tumor removal surgery to accurately delineate tumor margins. This precision would be crucial in surgeries aimed at preserving organs and in operations near critical structures. Techniques like fluorescence-guided surgery might employ biomarkers linked to fluorescent dyes, possibly illuminating cancer cells under special lighting conditions during surgery [17]. This could aid surgeons in real-time differentiation between cancerous and non-cancerous tissues, a feature especially beneficial in minimally invasive surgeries such as laparoscopic or robotic procedures. Additionally, these biomarkers might assist in preserving bladder function by ensuring that only cancerous tissues are removed, which could be critical for maintaining quality of life. They could guide targeted biopsies and intraoperative frozen section analysis, potentially helping confirm that surgical margins are free of cancer cells.

In this study, UHPLC-UHRMS was employed to investigate metabolic changes in a substantial sample size of 198 human tissue samples derived from 99 bladder cancer cases. The primary objective of this research was to identify the metabolites that distinguish cancerous tissues from normal tissues, while also enabling differentiation between different stages and grades of bladder cancer.

2. Materials and methods

2.1. Materials and equipment

All solvents were of at least LC-MS grade and were obtained from

Merck Life Science Sp.z.o.o (Darmstadt, Germany). Formic acid in LC-MS grade was purchased from Fisher Scientific GmbH Im (Schwerte, Germany). High-purity deionized water (> 18 MΩ·cm) was produced locally.

2.2. Collection of human tissue samples

Tissue samples were collected from 99 individuals with bladder cancer (79 males, 20 females, average age 72) undergoing surgical therapy at John Paul II Hospital in Kolbuszowa (Poland). The research was approved by the local Bioethics Committee at the University of Rzeszow (Poland, permit number 2018/04/10) and followed all current rules and regulations. All of the patients in this study were Caucasian. Patients' specimens and clinical data were acquired with their informed consent. The findings of all laboratory tests (complete blood count, bleeding profile, kidney function tests, and CRP) were all within normal levels. Tissues for the metabolomic investigation were obtained during a bladder tumor transurethral resection. We obtained about cubic fragments of 2–4 mm in size of the malignant tumor and a fragment of normal bladder mucosa for the metabolomic research. Both of these fragments were sliced in half, with one component examined and the other sent for histological testing to confirm the diagnosis. The samples were promptly frozen and stored at − 60°C until future use. Table 1 shows the pathological and clinical characteristics of the individuals.

2.3. Preparation of tissue metabolite extracts

As previously described, medium-to-high polarity metabolites were recovered from tissue samples [18]. In summary, a weighted amount of sectioned tissue (0.3–19 mg) was put into a 2 ml centrifuge tube, and a 1:2 MeOH/$CHCl_3$ (1:2, v/v, 90 µl/mg of tissue) solution was added and homogenized with borosilicate glass beads for 60 s. After that, each tube was homogenized twice for 60 s with a 5-minute pause interval in cold H_2O (12 µl/mg of tissue). The samples were incubated at − 20 degrees Celsius for 20 min before being centrifuged at 14,000xg for 10 min at 4 degrees Celsius to remove cells and other precipitated material. The polar (upper) phase was moved to a new 1.5 ml microcentrifuge tube, and the non-polar (lower) phase was similarly transferred. Finally, 20% of the volumes of the polar phase and the whole volume of non-polar phase samples were taken and used for UHPLC-UHRMS analysis with C18 and HILIC columns respectively. Using a SpeedVac-type vacuum concentrator (at 0.9 mbar) all samples were lyophilized to complete dryness. Due to the relatively big spread of tissue weights, dried polar extracts were dissolved in constant volume - 1100 µl of methanol, and the tissue weight normalization was performed in the MetaboScape program (version 2022b). Afterward, the mixtures were incubated at a temperature of 4 °C for 15 min. To separate any remaining particles, the solutions underwent centrifugation at 4 °C and 12,000 x g for 10 min. From the resulting solutions, volumes of 900 µl of polar extracts were transferred to HPLC vials. Vacuum-dried lower phases (low polar extracts) were dissolved in weight-normalized volumes of methanol (33.3 µl/mg of tissue). The vial, containing the extracted sample, was then positioned in the autosampler and introduced for analysis. All procedures involving human tissue samples were conducted in compliance with applicable standards under appropriate biosafety conditions. Personnel were equipped with standard PPE, including gloves and eye protection, and worked within designated biosafety cabinets. Chloroform was handled in a well-ventilated fume hood with appropriate PPE to prevent inhalation and skin contact, in accordance with applicable standards. All waste materials were disposed of following established protocols for biohazardous and chemical waste.

2.4. Analysis of tissue samples

Tissue extracts were analyzed using a Bruker Elute UHPLC system with Hystar 3.3 software and an ultra-high-resolution mass spectrometer Bruker Impact II (60,000 + resolution version; Bruker Daltonik GmbH) ESI QTOF-MS with Data Analysis 4.2 (Bruker Daltonik GmbH) and Metaboscape (ver. 2022b) as described in our previous publication [18]. A Waters UPLC column ACQUITY BEH (C18 silica, 1.7 µm particles, 50 ×2.1 mm) was used for separation and analysis of polar tissue extracts, while the HILIC column (1.7 µm particles 50 ×2.1 mm) was used for non-polar extract of tissues. Suitable column guards for all studies were employed for all analyses. RP C18 column was used with mobile phases: A = water with 0.1% formic acid, B = acetonitrile with 0.1% formic acid (v/v). Samples in the autosampler were thermostated at 4 °C, and a volume of 2 µl (5 µl for HILIC) of the extract was loaded onto the column at a flow rate of 200 µl/min, with 1% B. The percentage of B varied with time as follows: 0 min – 1%, 0.56 min - 1% B, 4.72 min - 99%, 5.56 min - 99%, 5.6 min – 1%, 9.45 min – 1%. The solvent flow was set at 450 µl/min, and the column was maintained at 40 °C. HILIC column was used with mobile phases: A = 95:5 acetonitrile: water (v/v) with 10 mM

Table 1
Participant characteristics.

	BC patients	
	Training set	Validation set
Number		
General	70	29
Male	56	23
Female	14	6
Age (mean/SD)	73(10)	71(10)
Grade[a]		
High grade	27	12
Low grade	39	16
LG (70%) and HG (30%)	0	1
LG (85%) and HG (15%)	1	-
PUNLMP	3	-
Stage		
pT1	13	5
pT2	7	3
pTa	50	21
Type of surgery		
TURBT	68	29
Cystectomy	2	0
Tumor origin		
Primary	40	18
Recurrent	30	11
Hematuria		
At diagnosis	69	29
At sampling	51	20
Tumor size [cm]		
< 1.9	51	9
2-3	3	10
> 3	15	6
Multifocal/flat	0	4
Multifocality		
0	1	0
1	50	21
2-3	7	5
> 3	12	3
Previous treatment		
BCG	10	4
neoadjuvant chemotherapy (cisplatin based)	2	0
Tumor histology		
Papillary	69	27
Flat, CIS	1	0
Solid, non-papillary	1	2
Tobacco smoking		
Non smoking	53	21
Currently smoking	9	3
Previous smoking	7	5

[a] Tumors were classified according World Health Organization (WHO)/International Society of Urological Pathology (ISUP) classification criteria; BC – bladder cancer; BCG - bacillus calmette guerin; CIS - carcinoma in situ; LG – low-grade; HG – high-grade; PUNLMP - papillary urothelial neoplasm of low malignant potential; pT1 and pTa – high risk non-muscle invasive bladder cancer; pT2 – muscle invasive bladder cancer; pT- the stage has been based on pathological or microscopic findings; SD: standard deviation.

ammonium acetate, B = 1:1 acetonitrile:water (v/v) with 10 mM ammonium acetate. Percentage of B varied with time as follows: 0 min – 0%, 6 to 7 min – 20%, 7.1 to 8 min – 0%. Internal calibration using 10 mM sodium formate (water: isopropanol 1:1 v/v) ions was automatically performed in Metaboscape, utilizing a syringe pump at an infusion flow rate of 0.12 ml/h, in high precision calibration (HPC) mode. Analyses in positive autoMSMS mode were conducted with specific parameters, including m/z range of 50–1200, capillary voltage of 4.5 kV, nebulizer pressure of 2.7 bar, dry gas flow of 12 L/min, drying gas temperature of 220 °C, hexapole voltage of 50 Vpp, funnel 1 and funnel 2 voltages of 200 Vpp, pre-pulse storage time of 5 μs, and transfer time of 60 μs. Collision-Induced Dissociation (CID) was employed with predetermined settings: absolute threshold (per 100 sum): 200 cts; absolute threshold 88 cts; active exclusion 3 spectra; release after 0.3 min, isolation mass: for $m/z = 100$, the width was 3, for 500 width was 4, for 1000 was 6 and for 1300 was 8); collision energy value was 30 eV. MS frequency was 20 Hz and MSMS from 5 to 30 Hz. Untargeted annotations were carried out in Metaboscape (ver. 2022b) with specific criteria for mass deviation ($\Delta m/z$) under 2 ppm and mSigma value under 20 to ensure accurate compound identification. For identification and molecular formula generation, the exact mass of parent ions was matched with < 3 ppm error and mSigma value < 50 in most cases. All the molecular formulas were obtained using the Smart Formula tool and the C, H, N, O, P, S, Cl, Br, I, and F elements. MSMS spectra were automatically matched against MSMS libraries, such as Bruker HMDB 2.0 library, MassBank of North America (MoNA) library [19], and NIST ver. 2020 MSMS library [20], to aid in compound identification. Quality control (QC) samples were regularly prepared from 10 different tissue extracts and measured every 10 samples throughout the analytical run to assess method stability and repeatability. All measurements were performed in technical triplicates to ensure data reliability and consistency. Data for replicates was managed by Bruker Metaboscape ver. 2022b. This program uses the Time aligned Region complete eXtraction (T-ReX) algorithm that extracts all relevant information, automatically and in a "region complete" manner. In cohorts of LC-QTOF-MS/MS data sets ions belonging to the same compound are combined, aligned across all samples, and automatically re-extracted in individual samples if initially below the peak picking threshold therefore addressing the missing value problem in statistics. For each m/z value in each sample, we calculated the mean value from the triplicate measurements. In cases where one or more of the triplicate measurements were missing or fell below the detection limit, we calculated the mean using the available data from the triplicates for that specific m/z value.

2.5. Statistical analysis

All metabolite datasets were analyzed using MetaboAnalyst version 5.0 online software [21]. The multivariate statistical analysis employed in this study is similar to that detailed in our recent papers [22,23]. In brief, the metabolite data from each analytical technique was log-transformed and auto-scaled. Unsupervised Principal Component Analysis (PCA) and Orthogonal Partial Least Squares Discriminant Analysis (OPLS-DA) were performed on the obtained metabolite profiles. Metabolites with Variable Importance in Projection (VIP) values more than 1.0, as determined by the OPLS-DA modeling, were regarded as potentially important discriminators of BC from AN tissue. Validation and accuracy of the OPLS-DA models were assessed using permutation tests with 2000 steps and 5-fold cross-validation. To assess the statistical significance of tissue metabolite level differences, a paired non-parametric t-test with Mann-Whitney and Bonferroni correction and paired fold change (FC) analysis was used. P-values and false discovery rates (FDR) less than 0.05, as well as FC > 2.0 or < 0.5, were considered statistically significant. The P-value and FDR corrections were applied across the entire list of identified metabolic features. Furthermore, receiver operating characteristic curve (ROC) evaluations using random forest modeling were done to validate the OPLS-DA models and assess the diagnostic value of the metabolites. Metabolite variables having an AUC (area under the curve) larger than 0.75 were judged important for distinguishing the BC versus AN tissue metabolome. Independent multivariate statistical analyses were performed on the training and validation metabolite datasets. External validation was performed using two independent datasets (hence referred to as the training and validation datasets) to evaluate the performance of the OPLS-DA models. Both the training and validation datasets were subjected to predefined statistical criteria. To identify metabolic pathways that are most likely impacted by bladder cancer, a metabolic pathway impact analysis was performed using MetaboAnalyst 5.0 [21] with the Kyoto Encyclopedia of Genes and Genomes [24] for Homo sapiens and quantitative pathway enrichment analysis with the Small Molecule Pathway Database (SMPD), We used a one-way analysis of variance (ANOVA) with Tukey's post-hoc testing to see if there were any significant differences in average math test results between different stages and grades of BC.

3. Results

In this study, we characterized the metabolic profile of cancer and normal tissue extracts from 99 patients diagnosed with BC to identify the compounds that most differentiate the bladder cancer tissue (BCT) from the adjacent tissue (ANT). Following the extraction of tissue samples, we obtained two distinct fractions – polar and low-polar one. To analyze these fractions effectively, we employed a C18 column for the polar fraction and a HILIC column for well-controlled retention of the low polar compounds of the low polar fraction. From both measurements, two distinct datasets were created: a training set consisting of 70% of all samples and a validation set containing the remaining 30% of samples. Subsequently, tissue metabolic profiling was conducted separately on these two datasets. The training dataset was utilized to identify tissue markers that differentiate between ANT and BCT and also both high-grade and low-grade BCT. The validation dataset was employed to independently validate the diagnostic performance of tissue metabolite biomarkers. However, when analyzing samples from different stages of cancer, as well as different age and gender groups, the number of available samples was insufficient to carry out a reliable statistical analysis when dividing them into two independent sets. Consequently, the study was performed using the entire dataset as a whole. Clustering of QC samples prepared from bladder tissue extracts measured on HILIC and C18 columns is presented as PCA plots in the supplementary data in Fig. S1.

3.1. Distinguishing between normal tissue and bladder cancer

A total of 1999 m/z features were identified using a HILIC column, while 659 m/z features were detected using a C18 column in each tissue sample. These features were required to be present in at least nine samples corresponding to the smallest group of cancer subtypes. The dataset obtained from the HILIC and C18 columns was partitioned into separate training and validation sets. Subsequently, multivariate statistical analysis was performed on these datasets using the MetaboAnalyst v 5.0 platform.

For the tissue extract data obtained from the C18 column, the unsupervised PCA analysis revealed a partial separation between BCT and ANT samples. The first two principal components (PC1 and PC2) accounted for 75.0% and 4.6% of the total variance, respectively, demonstrating a significant degree of group separation in the training set. Outliers were sparsely distributed within the central 95% of the field of view, as depicted in Fig. 1A. Furthermore, in the validation set, PC1 (66.8%) and PC2 (7.3%) exhibited the most prominent separation between BCT and ANT samples, as shown in Fig. S2A of the supplementary information.

To elucidate the metabolic distinctions between the BCT and ANT groups, a supervised OPLS-DA analysis was employed. The score plot

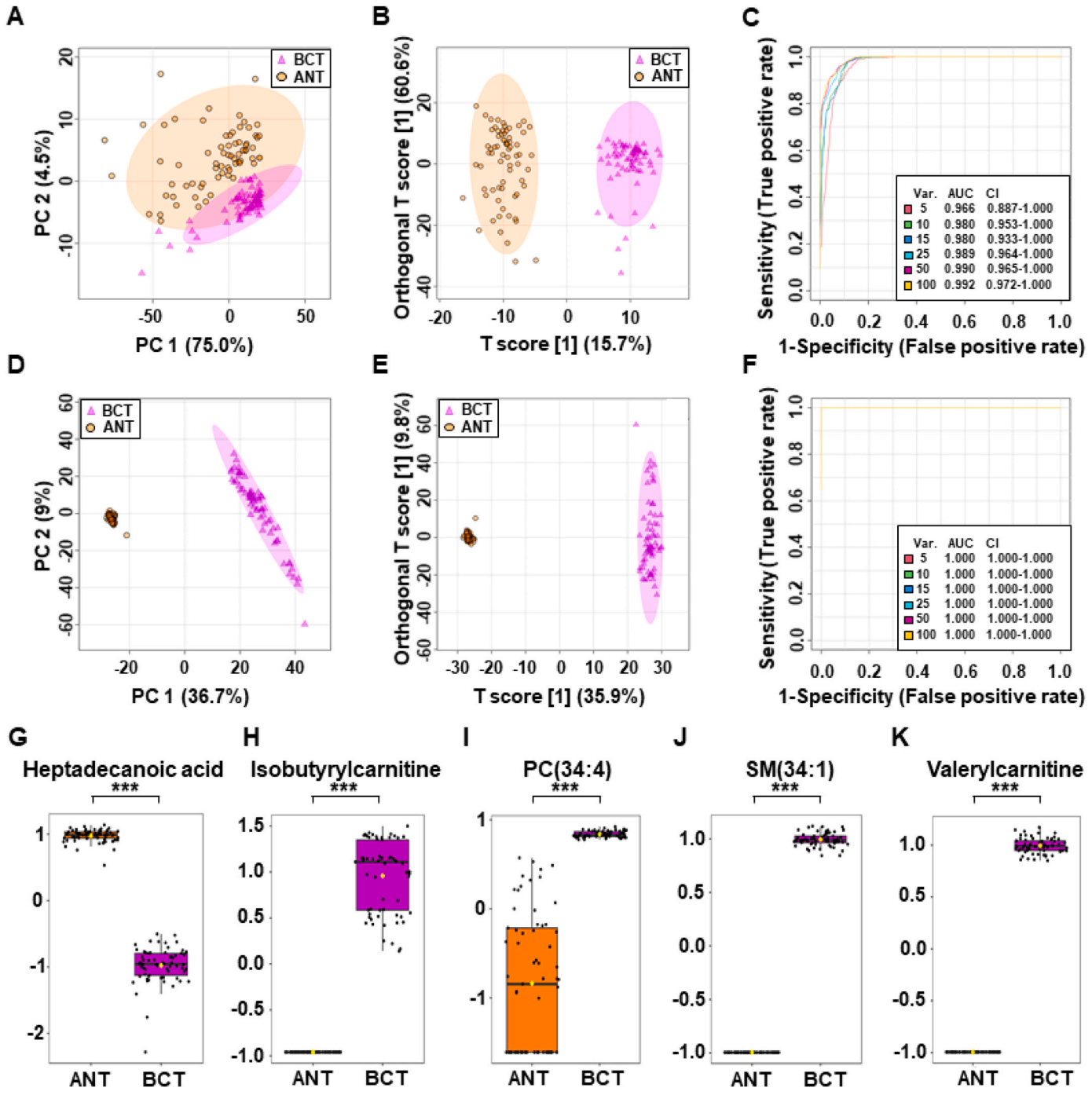

Fig. 1. Analysis of BCT and ANT metabolite profiles in the training set. (A) 2D PCA and (B) OPLS-DA scores plots and (C) ROC curves of the BCT (violet) and ANT (orange) samples obtained using column C18; (D) 2D PCA and (E) OPLS-DA scores plots and (F) ROC curves of the BCT (violet) and ANT (orange) samples obtained using column HILIC; (G-K) Box-whisker plots of selected metabolites levels in tissue samples from BCT and ANT.

generated from the training set exhibited a clear demarcation between the two groups, as illustrated in Fig. 1B. To validate the OPLS-DA model, 5-fold cross-validation and 2000 permutation tests were conducted (refer to Table S1 in the supplementary information). Notably, the results indicated robust discrimination between the groups, with a Q^2 value of 0.921, an R^2Y value of 0.954, and an extremely low P-value of 5E-04 (0/2000). These findings underscore the presence of significant metabolic variations between BCT and ANT samples. The OPLS-DA model demonstrated high interpretability and predictability, as evidenced by its elevated R^2Y and Q^2 values. Consistently, the validation set's OPLS-DA model exhibited a similar ability to discriminate between BCT and ANT, with excellent permutation test outcomes (Q^2 =0.901, R^2Y=0.989, p-value 5E-04 (0/2000)). The VIP plot, derived from the OPLS-DA model, served as a valuable tool for identifying potential tissue biomarkers associated with BC. To evaluate the statistical significance of metabolite level differences, a comprehensive analysis was conducted, employing paired fold change analysis, paired non-parametric t-tests (Mann-Whitney), and Bonferroni correction. Subsequently, univariate ROC analysis was performed on both the training and validation sets to assess the diagnostic capability of the models, as depicted in Fig. 1C. The area under the ROC curve (AUC), a reliable indicator of model performance, was utilized as a metric to evaluate the sensitivity and specificity

of the identified biomarkers. By integrating VIP scores (> 1.0), t-tests (FDR and P-values < 0.05), fold change (FC > 2.0 or < 0.5), and AUC (> 0.75) analyses from both the training and validation sets, a total of nine metabolites were identified as significant discriminators between BCT and ANT tissue. Among the *m/z* values that met the statistical criteria in both the training and validation sets, our focus was solely on those that corresponded to specific compounds with confirmed structures. Moreover, only metabolites naturally occurring in the human body were considered for further analysis and interpretation. These significant metabolites are listed in Table 2.

A similar analysis was performed on data obtained using the HILIC column. The PCA analysis revealed a clear separation of BCT and ANT. The first two principal components (PC1 and PC2) accounted for 36.7% and 9% of the total variance, indicating significant group separation in

Table 2
Differential metabolites for discrimination between BCT and ANT (P-value and FDR < 0.001; VIP > 1; FC < 0.5 and > 2; AUC > 0.8).

No.	Name	Column type	Formula	*m/z*[a]	RT [s]	VIP[b]	FC[c]	P-value[d]	FDR[d]	AUC[e]	Spec. [%][e]	Sens. [%][e]
1	Heptadecanoic acid[f,h,i]	HILIC	$C_{17}H_{34}O_2$	288.2894	46	1.63	0.0	2.5E-12	1.3E-11	1.000	100	100
2	Isobutyrylcarnitine[f,h,i]	HILIC	$C_{11}H_{21}NO_4$	232.1542	404	1.61	16.6	2.5E-12	1.3E-11	1.000	100	100
3	PC(34:4)[f,h,i]	HILIC	$C_{42}H_{76}NO_8P$	754.5356	238	1.40	84.1	2.5E-12	1.3E-11	1.000	100	100
4	SM(34:1)[f,h,i]	HILIC	$C_{39}H_{79}N_2O_6P$	703.5744	307	1.67	5.7	2.5E-12	1.3E-11	1.000	100	100
5	Valerylcarnitine[f,h,i]	HILIC	$C_{12}H_{23}NO_4$	246.1698	384	1.67	5.7	2.5E-12	1.3E-11	1.000	100	100
6	Hypoxanthine[f,h,i]	HILIC	$C_5H_4N_4O$	137.0456	67	1.41	0.0	2.5E-12	1.3E-11	0.998	65	75
7	C17 Sphinganine[f,h,i]	C18	$C_{17}H_{37}NO_2$	288.2895	214	1.16	0.4	2.7E-09	9.8E-09	0.815	79	80
8	C17 Sphingosine[f,h,i]	HILIC	$C_{17}H_{35}NO_2$	286.2739	28	1.34	0.0	2.5E-12	1.3E-11	0.995	91	99
9	PC(38:3)[f,h,i]	HILIC	$C_{46}H_{86}NO_8P$	812.6133	227	1.32	113.7	3.6E-12	1.5E-11	0.987	92	92
10	Ortophosphate[f,i]	HILIC	H_3O_4P	98.9839	26	1.42	0.0	2.5E-12	1.3E-11	0.986	95	95
		C18	H_3O_4P	98.9840	28	1.42	0.3	4.8E-12	7.0E-11	0.886	80	90
11	Inosine[f,g,h,i]	HILIC	$C_{10}H_{12}N_4O_5$	269.0879	81	1.35	30.9	2.7E-12	1.3E-11	0.979	97	92
12	Iminodiacetic acid[f,i]	HILIC	$C_4H_7NO_4$	134.0446	165	1.51	0.0	1.1E-11	3.6E-11	0.969	100	94
13	Uracil[f,i]	HILIC	$C_4H_4N_2O_2$	113.0344	33	1.19	0.1	1.8E-11	5.2E-11	0.962	99	89
14	PC(36:5)[f,h,i]	HILIC	$C_{44}H_{78}NO_8P$	780.5531	227	1.36	58.0	5.2E-12	1.9E-11	0.950	99	92
15	8,11,14-Eicosatrienoylethanolamide[f,h,i]	HILIC	$C_{22}H_{39}NO_2$	350.3050	29	1.38	0.0	1.0E-11	3.3E-11	0.931	89	97
16	PC(16:1/16:1)[f,h,i]	HILIC	$C_{40}H_{76}NO_8P$	730.5379	237	1.29	32.3	8.2E-12	2.7E-11	0.923	99	91
17	PC(34:1)[f,h,i]	HILIC	$C_{42}H_{82}NO_8P$	760.5846	234	1.01	0.1	3.5E-09	7.1E-09	0.904	94	85
18	Glycerophosphocholine[f,g,h,i]	C18	$C_8H_{20}NO_6P$	258.1100	21	1.87	67.9	2.7E-11	2.5E-10	0.893	83	93
19	PC(40:6)[f,h,i]	HILIC	$C_{48}H_{84}NO_8P$	834.6004	221	1.20	47.4	6.1E-11	1.6E-10	0.887	88	80
20	LPC(18:2)[f,h,i]	HILIC	$C_{26}H_{50}NO_7P$	520.3393	321	1.17	28.8	1.7E-10	4.1E-10	0.877	99	82
21	5-Dodecenoic acid[f,g,h,i]	C18	$C_{12}H_{22}O_2$	199.1692	234	1.35	0.4	1.5E-11	1.6E-10	0.871	86	81
22	PC(18:0e)[f,h,i]	HILIC	$C_{26}H_{54}NO_7P$	524.3701	331	1.05	6.4	1.6E-10	4.0E-10	0.865	94	83
23	Palmitoleoylethanolamide[f,h,i]	C18	$C_{18}H_{35}NO_2$	298.2738	236	1.32	0.4	5.6E-11	4.4E-10	0.850	83	80
24	Hydrocinnamic acid[f,g,h,i]	C18	$C_9H_{10}O_2$	151.0752	132	1.21	0.4	3.3E-10	1.7E-09	0.833	80	79
25	Sorbose[f,g,h]	C18	$C_6H_{12}O_6$	203.0526	22	1.20	0.4	3.4E-09	1.2E-08	0.823	86	81

SM: sphingomyelin; VIP: variable influence on projection
[a] Experimental monoisotopic mass of ion;
[b] VIP scores derived from OPLS-DA model;
[c] fold change between cancer and control tissue extract calculated from the abundance mean values for each group – cancer-to-normal ratio;
[d] Derived from paired non-parametric t-test;
[e] ROC curve analysis for individual biomarkers;
[f] the metabolites identified by high precursor mass accuracy;
[g] the metabolites identified by matching retention time;
[h] the metabolites identified by matching isotopic pattern;
[i] the metabolites identified by matching MS/MS fragment spectra; AUC: area under the curve; FC: fold change; FDR: false discovery rate; LPC: lysophosphatidylcholine; *m/z*: mass-to-charge ratio; PC: phosphatidylcholine; RT: retention time; Sens.: Sensitivity; Spec.: Specificity;

the training set. As seen in Fig. 1D, outliers were sparsely dispersed inside the middle 95% of the field of vision. Furthermore, as shown in Fig. S2D of the supplementary information, PC1 (37.4%) and PC2 (8.1%) demonstrated the most noticeable separation between BCT and ANT samples in the validation set. The OPLS-DA score plots generated for both the training and validation sets demonstrated exceptional differentiation between the two groups, as depicted in Fig. 1B and Figure 1SB (supplementary material). The 5-fold cross-validation and permutation test were performed to validate the OPLS-DA model (refer to Table S2 in the supplemental information). Notably, the results showed strong group discrimination, with a Q^2 value of 0.997, an R^2Y value of 0.998, and a low P-value of 5E-04 (0/2000). These data highlight the existence of significant metabolic differences between BCT and ANT samples. A comprehensive analysis was conducted to determine the statistical significance of metabolite level differences. This analysis included, additionally, paired fold change analysis, paired non-parametric t-tests (Mann-Whitney), and Bonferroni correction and univariate ROC analysis (Fig. 1F, S1F) was performed on both the training and validation sets to evaluate the statistical significance of metabolite level differences and the diagnostic capacity of the models. Using the same statistical criteria as before (VIP $>$ 1.0), FDR and P-values $<$ 0.05, FC $>$ 2.0 or $<$ 0.5, and AUC $>$ 0.75) from both the training and validation sets, a total of twenty-five metabolites were identified as significant discriminators between BCT and ANT tissue using HILIC column. These significant metabolites are listed in Table 2.

These findings suggest that in total, twenty-five metabolites may have enhanced diagnostic potential and could be valuable indicators of malignant versus normal tissues of patients with bladder cancer when evaluated together.

3.2. Distinguishing between grades of bladder cancer

To evaluate the potential of tissue extract metabolite profiles in distinguishing between different grades of BCT and ANT, we conducted a multivariate statistical analysis on separate training and validation datasets. The analysis involved 96 tissue samples obtained from patients diagnosed with high-grade (HG) and low-grade (LG) cancer, excluding three samples from patients with papillary urothelial neoplasm of low malignant potential (PUNLMP). We used the training dataset, comprising 26 HG BCT and HG ANT samples, along with 39 LG BCT and LG ANT samples. To verify the reliability and consistency of the distinct group clustering observed in the PCA model, we employed the validation dataset comprising 12 HG BCT and ANT samples and 16 LG BCT and ANT samples.

In both the training and validation datasets obtained using the HILIC and C18 column, the PCA and OPLS-DA scores plots demonstrated clear differentiation between HG BCT and ANT groups, as depicted in Fig. S3 A-D of the supplementary material. The OPLS-DA models were validated using a 5-fold cross-validation and permutation test, demonstrating robust group discrimination. The results exhibited strong performance, with a Q^2 value exceeding 0.960, an R^2Y value surpassing 0.865, and a very low P-value of 5E-04 (0/2000) (Table S1, supplementary material). Additional analyses such as ROC analysis, paired no-parametrical t-test, and fold change analysis were conducted. These assessments, along with careful consideration of statistical parameters (VIP $>$ 1, *P*-value, FDR $<$ 0.05, FC $<$ 0.5 or $>$2.0, AUC $>$ 0.70) led to the identification of 26 specific compounds. These compounds exhibited the highest potential for distinguishing cancerous tissue from normal tissue in patients diagnosed with HG BC (Table S2, supplementary data).

Similar analyses were conducted on tissue extracts collected from patients diagnosed with LG BC. The PCA and OPLS-DA scores plots in both the training and validation datasets produced using the HILIC and C18 column exhibited clear differences between the LG BCT and LG ANT groups, as shown in Fig. S3 E-H of the supplemental material. A validation of the OPLS-DA models, revealing robust group discrimination. The results were strong, with a Q^2 value greater than 0.959, an R^2Y value greater than 0.821, and an extremely low P-value of 5E-04 (0/2000) (Table S1, supplemental material). Following that, additional analyses were performed, including ROC analysis, paired no-parametrical t-test, and FC analysis. These evaluations, combined with careful consideration of statistical characteristics (VIP $>$ 1, P-value, FDR 0.05, FC 0.5 or $>$ 2.0, AUC $>$ 0.70), resulted in the discovery of 24 distinct compounds. In individuals with LG BC, these metabolites have the greatest potential for differentiating malignant cells from normal tissue. Unfortunately, comparing the three cancer grade groups (HG BCT versus LG BCT) revealed no statistically significant differences (data not shown).

3.3. Distinguishing between different stages of bladder cancer

A metabolomics analysis of tissue samples was also performed to see if distinct metabolite patterns can help distinguish between stages of BC. On a total of 198 tissue extracts from 71 patients with pTa BC, 18 patients with pTa BC, and 10 patients with pT2 BC, we performed PCA, OPLS-DA, ROC analysis, non-parametric paired t-test, and FC analysis. However, due to the limited availability of patients with pT1 and pT2 malignancy, the analysis was carried out without stratification into training and validation sets. The obtained datasets from both the HILIC and C18 columns were subjected to analysis. In both cases, the PCA and OPLS-DA scores plots clearly exhibited distinct separation between the pTa, pT1, and pT2 stages of cancer tissues and their corresponding adjacent normal tissues. These findings are visually represented in Fig. S4 of the supplementary material. A validation of these OPLS-DA models, demonstrates strong predictive power, accurately distinguishing between the different groups with a Q^2 value greater than 0.976 and a high level of accuracy in capturing the variance in the dataset with, an R^2Y value greater than 0.894 (Table S1, supplementary material). Based on the cut-off criteria (FC $>$ 2 or $<$ 0.5, VIP $>$ 1; AUC $>$ 0.75, *P*-value and FDR $<$ 0.05), finally, 26, 30, and 33 metabolites appeared to be most relevant for sample distinction between pTa BCT vs. pTa ANT, pT1 BCT vs. pT1 ANT and pT2 BCT vs. pT2 ANT, respectively (Table S3, supplementary material). Unfortunately, comparing the three cancer stage groups (pT1 BCT versus pTa BCT versus pT2 BCT) revealed no statistically significant differences (data not shown). LC-MS data for all identified compounds are provided in Table S4 of supplementary data.

3.4. Pathway analysis of potential biomarkers

MetaboAnalyst 5.0 was utilized to conduct a metabolic pathway impact analysis, with the goal of identifying the key pathways implicated in the observed alterations in tissue metabolite levels. Pathway and quantitative pathway enrichment analyses were performed on a set of 41 compounds that played a crucial role in distinguishing BCT and ANT. Notably, these analyses also considered the compounds that exhibited significant differences across various stages and grades of BC. Out of the 41 compounds examined, a total of 40 compounds were found to be relevant to human metabolism. Leveraging the KEGG (Kyoto Encyclopedia of Genes and Genomes) database, the pathway analysis revealed 13 pathways specifically associated with BC. Among these identified pathways, four were found to be particularly significant: glycerophospholipid metabolism, purine metabolism, pyrimidine metabolism, and linoleic acid metabolism. These findings are illustrated in Fig. 2A and detailed in Table S5 of the supplementary information.

To broaden the investigation of BC-related pathways in our metabolomic study, we performed a quantitative enrichment analysis using the pathway enrichment module of MetaboAnalyst 5.0, utilizing the Small Molecule Pathway Database (SMPDB). Through this analysis, a comprehensive set of 59 pathways associated with BC was identified. Among these pathways, two additional pathways emerged as particularly significant: lactose synthesis and glycolysis. These findings, visually represented in Fig. 2B and detailed in Table S6 of the supplementary information, provide crucial insights into the metabolic processes

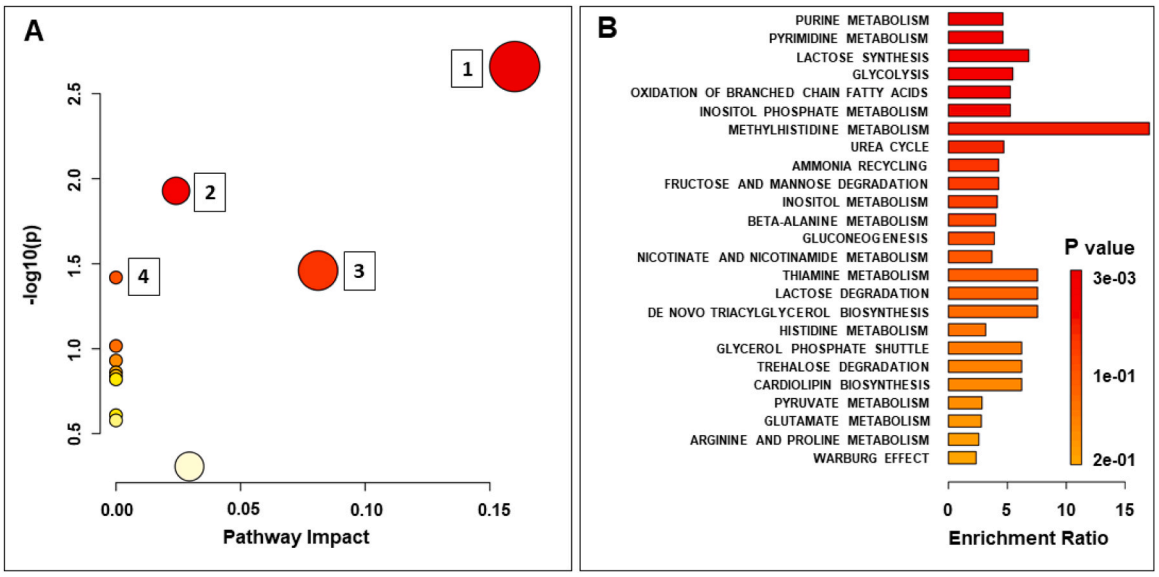

Fig. 2. Analysis of the topology of selected statistically significant tissue metabolites in BC. (A) Pathway analysis based on KEGG, with bubble area corresponding to the impact of each pathway and color representing significance from red to white, from greatest to least. (1) Glycerophospholipid metabolism; (2) Purine metabolism; (3) Pyrimidine metabolism; (4) Linoleic acid metabolism; (B) Quantitative enrichment analysis based on SMPDB. KEGG: Kyoto Encyclopedia of Genes and Genomes; SMPDB: The Small Molecule Pathway Database.

underlying bladder cancer development and progression.

4. Discussion

In this study, our primary objective was to employ untargeted metabolic profiling to investigate tissue extracts obtained from 99 patients diagnosed with BC. Our aim was to uncover distinctive metabolic signatures that could serve as potential biomarkers for early and accurate detection of BC, utilizing the UHPLC-UHRMS technique. To accomplish this, we conducted an untargeted analysis of both ANT and BCT, seeking to identify a panel of metabolites that exhibited differential abundance between the two tissue types. Through our analysis, we successfully identified 25 metabolites. Notably, 12 of these compounds were found to be present at higher levels in cancer tissue compared to adjacent normal tissue, while 13 compounds were present at lower concentrations. The elevated levels of these 12 metabolites could potentially indicate increased synthesis of tumor-related metabolites, which may be secreted by cancer cells or result from alterations in the composition of non-cancerous tissues due to tumor infiltration through the epithelial barrier. Moreover, the presence of tumors could trigger inflammatory responses, contributing to the observed elevation of certain metabolites.

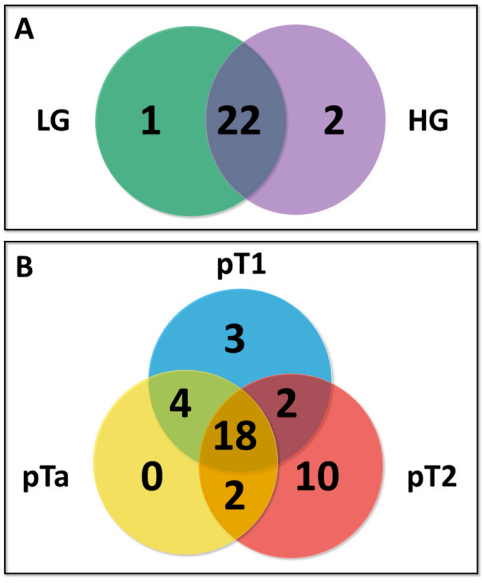

Fig. 3. Venn diagrams illustrate the number of tissue metabolites common and unique in different (A) grade and (B) stages of BC.

Our research utilized the UHPLC-HRMS method to compare urine and serum profiling results in bladder cancer (BC) patients [22,25]. In this study, we focused on investigating tissue biomarkers to complement information obtained from serum and urine biomarkers. Our findings reveal that changes in tumor tissues can significantly affect the composition of metabolites in the blood and urine. However, these correlations are often complex and not always direct, with some biomarkers only detectable in tissue, particularly in early cancer stages.

One key discovery was the markedly elevated level of valerylcarnitine in cancerous tissue extracts, showing 100% specificity and sensitivity, a finding corroborated in blood serum [25] and contrasted by decreased levels in urine [22]. The same class of compounds also includes isobutyrylcarnitine, which also turned out to be an excellent tissue marker with 100% specificity and sensitivity. Valerylcarnitine and isobutyrylcarnitine, both acylcarnitines, play crucial roles in fatty acid metabolism and energy production, and their altered levels are indicative of the cancer cells' aberrant metabolism, commonly referred to as the Warburg effect [26]. This effect leads to an accumulation of specific metabolites, like valerylcarnitine, in cancer cells and consequently in the tissues, with potential implications for cancer diagnosis and treatment [27]. The elevated levels of valerylcarnitine in serum could be due to the release of this metabolite from the tumor tissues into the bloodstream. As tumor cells proliferate and metabolize, they may release more of certain metabolites as a byproduct of their increased metabolic activities. Previous research has indicated elevated levels of carnitines in bladder cancer tumor tissues. Several studies have investigated the metabolomic profiles of BC and identified dysregulated metabolites, including carnitines. For instance, a study conducted by Putluri et al. [11], analyzed the metabolomic profiles of BC tissues using liquid chromatography-mass spectrometry (LC-MS). The findings of this study revealed that carnitine levels were significantly elevated in bladder cancer tumor tissues when compared to adjacent benign and normal

tissues. Similarly, subsequent examination of the metabolic profile of urine samples from BC patients indicated elevated levels of carnitines such as acetylcarnitine and isovalerylcarnitine in the urine of BC patients compared to controls [28–30]. These findings suggest that alterations in carnitine metabolism are associated with bladder cancer development and progression.

Another compound that was related to our previous results was the lipid PC(18:0) a specific type of phosphatidylcholine (PC), which is a major class of phospholipids and a crucial component of cell membranes. Our results indicated that PC(18:0) was present in significantly higher amounts in tumor tissues compared to adjacent normal tissues (FC = 6.4), and in lower amounts in serum from the same BC patients compared to the control group (FC = 0.69) [25]. Apart from PC(18:0), 11 other lipids belonging to the PC class were found to be significantly associated with cancer tissues, of which, interestingly, as many as 6 were significantly changed only in patients with pT2 stage of bladder cancer (Table 3). Among these compounds, PC(34:4) had the highest diagnostic ability with 100% specificity and sensitivity (Table 2). Phosphatidylcholines, including PC(18:0), are integral in maintaining membrane integrity, and fluidity, and in facilitating signal transduction processes. Aberrant membrane choline phospholipid metabolism (MCPM) is a hallmark of cancer cells, leading to altered levels of choline-containing metabolites like choline, phosphocholine, glycerophosphocholine, and phosphatidylcholine. These alterations are driven by the activation of biosynthetic enzymes such as choline kinase, and catabolic enzymes like phospholipases A, C, and D [31]. In bladder cancer, particularly, the phospholipase C (PLC) pathway, among others, is notably affected, contributing to abnormal gene regulation and tumor development. This dysregulation is implicated in the malignant transformation in various cancers, making these enzymes potential targets for anticancer chemotherapies [32]. Our findings align with the research by Tripathi et al. [12], which revealed elevated levels of phosphatidylcholine and other choline-containing compounds in tumor tissues compared to benign tissues. Similar dysregulation in phosphatidylcholines has been observed in other studies, further confirming the disrupted MCPM in bladder cancer [33]. This dysregulation may be reflected in the altered lipid metabolism of cancer cells. In cancerous tissues, there is an increased activity of lipid synthesis to support the rapid proliferation of cancer cells, potentially leading to the accumulation of compounds like PC(18:0). Conversely, the exchange of phospholipids such as PC(18:0) between cell membranes and blood may be impaired in cancer cells, leading to lower levels of PC(18:0) in the serum. Additionally, bladder cancer can influence local blood flow and substance distribution, causing variations in metabolite concentrations between tumor sites and the bloodstream. This complex interplay underscores the significance of PC(18:0) as a potential biomarker and a participant in the

Table 3
Differential metabolites for discrimination in all groups (P-value and FDR < 0.001; AUC > 0.8).

No.	Name	BCT vs. ANT		LG BCT vs. ANT		HG BCT vs. ANT		pTa BC vs. ANT		pT1 BC vs. ANT		pT2 BC vs. ANT	
		VIP	FC	VIP	FC	VIP	FC	VIP	FC	VIP	FC	VIP	FC
1	3-Methylhistidine	-	-	-	-	-	-	-	-	-	-	1.06	0.117
2	5-Dodecenoic acid	1.35	0.379	1.35	0.377	1.32	0.379	1.36	0.370	1.26	0.295	-	-
3	8,11,14-Eicosatrienoylethanolamidef	1.38	0.033	1.35	0.036	1.35	0.048	1.33	0.041	1.53	0.052	1.06	0.048
4	Acetylcarnitine	-	-	1.07	0.055	-	-	1.01	0.071	-	-	1.09	0.115
5	Adenine	-	-	1.55	119.690	1.56	207.540	1.55	126.760	1.54	171.430	1.53	138.940
6	C17-Sphinganine	1.16	0.442	-	-	1.06	0.461	-	-	1.17	0.330	-	-
7	C17-Sphingosine	1.34	0.031	1.33	0.028	1.29	0.040	1.34	0.033	1.32	0.039	1.36	0.024
8	Glycerophosphocholine	1.87	67.856	1.74	9.577	1.57	27.991	1.81	9.318	1.32	20.114	-	-
9	Heptadecanoic acid	1.63	0.003	1.63	0.003	1.59	0.003	1.63	0.003	1.61	0.003	1.55	0.003
10	Hydrocinnamic acid	1.21	0.432	1.21	0.423	1.2	0.430	1.22	0.418	1.19	0.341	-	-
11	Hypoxanthine	1.41	0.013	1.41	0.010	1.37	0.022	1.4	0.014	1.43	0.008	1.33	0.029
12	Iminodiacetic acid	1.51	0.020	1.47	0.020	1.51	0.021	1.46	0.021	1.38	0.034	1.48	0.049
13	Inosine	1.35	30.883	1.34	32.208	1.33	25.262	1.32	29.105	1.26	13.671	1.34	32.877
14	Isobutyrylcarnitine	1.61	16.593	1.6	16.010	1.56	16.636	1.59	15.049	1.56	17.967	1.51	11.719
15	LPC(18:2)	1.17	28.845	1.09	16.960	1.29	51.270	1.19	22.118	1.09	20.026	1.07	19.064
16	Oleamide	-	-	-	-	-	-	-	-	-	-	1.03	2.910
17	Ortophosphate	1.42	0.015	1.41	0.016	1.39	0.334	1.42	0.013	1.52	0.010	1.26	0.023
18	Palmitamide	-	-	-	-	-	-	-	-	1.04	0.158	-	-
19	Palmitoleoylethanolamide	1.32	0.380	1.32	0.381	1.26	0.386	1.35	0.364	1.17	0.326	1.08	8.400
20	Palmitoylcarnitine	-	-	-	-	-	-	-	-	-	-	1.08	8.353
21	PC(16:0/16:0)	-	-	-	-	-	-	-	-	-	-	1.09	3.435
22	PC(16:1/16:1)	1.29	32.284	1.26	29.925	1.33	34.979	1.29	34.072	1.21	13.062	1.32	30.346
23	PC(18:0e)	1.05	6.393	-	-	1.15	6.764	1.04	6.916	-	-	1.26	6.715
24	PC(30:0)	-	-	-	-	-	-	-	-	-	-	1.04	4.811
25	PC(34:1)	1.01	0.057	-	-	-	-	-	-	1.06	0.096	1.15	0.172
26	PC(34:4)	1.4	84.147	1.38	79.115	1.42	79.586	1.4	89.443	1.4	41.755	1.41	65.550
27	PC(35:2)	-	-	-	-	-	-	-	-	-	-	1.26	32.427
28	PC(36:3)	-	-	-	-	-	-	-	-	-	-	1.1	10.819
29	PC(36:5)	1.36	57.985	1.31	50.443	1.39	75.985	1.34	53.697	1.26	45.363	1.36	60.950
30	PC(38:3)	1.32	113.740	1.29	73.122	1.38	162.680	1.3	100.260	1.3	64.000	1.36	138.300
31	PC(40:6)	1.2	47.412	1.08	30.398	1.36	89.348	1.16	40.833	1.24	20.093	1.26	54.511
32	PC(O-34:1)	-	-	-	-	-	-	-	-	-	-	1.03	7.846
33	PC(O-36:5)	-	-	-	-	-	-	-	-	-	-	1.26	51.256
34	Propionylcarnitine	-	-	-	-	-	-	-	-	1.3	0.000	-	-
35	SM(34:1)	1.67	5.710	1.66	5.687	1.62	5.508	1.66	5.657	1.64	5.633	1.57	5.500
36	Sorbose	1.2	0.429	1.18	0.410	1.41	0.469	1.18	0.419	1.26	0.337	1.45	0.476
37	Stearoylcarnitine	-	-	-	-	-	-	-	-	-	-	1.14	14.060
38	Uracil	1.19	0.071	-	-	-	-	-	-	1.31	0.068	1.16	0.089
39	Valerylcarnitine	1.67	5.669	1.66	5.630	1.62	5.682	1.66	5.733	1.64	5.520	1.57	5.498

[a]VIP scores derived from the OPLS-DA model;
[b]fold change between cancer and control tissue extract calculated from the abundance mean values for each group – cancer-to-normal ratio; AUC: area under the curve; FC: fold change; FDR: false discovery rate; LPC: lysophosphatidylcholine; *m/z*: mass-to-charge ratio; PC: phosphatidylcholine; SM: sphingomyelin; VIP: variable influence on projection

pathophysiology of bladder cancer.

Another compound that was linked to our earlier research on the same group of patients was palmitoleoylethanolamide (PEA). PEA was significantly lower in extracts from cancerous tissues compared to adjacent healthy tissues, and conversely, its levels were significantly higher in the serum of BC patients than in the control group. This pattern can be attributed to the distinct metabolic behaviors of cancer cells. Unlike normal cells, cancer cells often have altered lipid metabolism, which could lead to the depletion of PEA in tumor tissues due to its higher consumption by rapidly growing cancer cells.

Our research has shown that, in addition to isobutyrylcarnitine and valerylcarnitine, the excellent ability to distinguish healthy tissue from the adjacent normal tissue with an AUC value of 1.0, indicating 100% specificity and sensitivity is demonstrated by three other lipids: PC (34:4), SM(34:1) and heptadecanoic acid. SM(34:1) is a sphingomyelin molecule involved in cell signaling and membrane fluidity. It's linked to diseases like cancer and has been associated with drug resistance and cancer progression, including cell proliferation and apoptosis. Several prior studies have consistently reported increased levels of various sphingomyelin species in both BC cell lines [34] and the urine of individuals diagnosed with bladder cancer [29]. Heptadecanoic acid, a saturated fatty acid with 17 carbon atoms, was found in lower amounts in cancerous tissues compared to healthy ones. Naturally present in dairy, meats, and certain oils, it serves as an energy source and is a component of lipids like triglycerides and phospholipids in cell membranes. Heptadecanoic acid has been previously identified as a potential cancer biomarker. For example, findings from the analysis of tissue samples from 66 patients with invasive ovarian carcinomas and 9 patients with borderline tumors of the ovary indicated that saturated fatty acids, including heptadecanoic acid, exhibited significant reductions in invasive ovarian carcinomas compared to ovarian borderline tumors [35]. In relation to the BC a study conducted by Pasikanti et al. [36] using two-dimensional gas chromatography time-of-flight mass spectrometry (GC×GC−ToFMS) revealed elevated levels of heptadecanoic acid in the urine of BC patients compared to controls.

A comprehensive analysis identified 23 differential metabolites that hold promise as potential markers for distinguishing between LG BCT and ANT (Table 3, S2, supplementary data). Among these metabolites, adenine, heptadecanoic acid, hypoxanthine, isobutyrylcarnitine, PC (34:4), SM(34:1), and valerylcarnitine exhibited the highest levels of specificity and sensitivity, making them the most distinguishing compounds in this model. Apart from heptadecanoic acid and hypoxanthine other compounds were identified in significantly higher levels in the BCT compared to ANT. Also, twenty-four differential metabolites were identified as a potential marker for discriminating between HG BCT and ANT. Among these metabolites, 5 had tremendous discriminant significance with the highest AUC, including heptadecanoic acid, isobutyrylcarnitine, PC(34:4), SM(34:1), and valerylcarnitine.

Interestingly, most metabolites that distinguished cancerous from healthy bladder tissue were common to both LG and HG bladder cancer patients. Acetylcarnitine uniquely differentiated cancerous from healthy tissues only in LG patients, being notably lower in cancerous tissues. Only in HG bladder cancer patients, C17-sphinganine was identified in significantly lower amounts, while PC(18:0e) was found in substantially higher levels in tumor tissues compared to adjacent healthy tissues.

Our study demonstrates that a tissue-based metabolite profile can effectively distinguish between different stages of bladder cancer (pTa, pT1, and pT2), as well as normal tissue (Table S3, supplementary data). Specifically, we identified 24 differentiating compounds in the tissue of pTa stage patients, 27 compounds in pT1 stage patients, and 32 compounds in pT2 stage patients, all exhibiting an area under the curve (AUC) greater than 0.804. These findings highlight the potential of these metabolites as robust indicators for accurately characterizing the various stages of bladder cancer. In the analysis of different stages of BC, most metabolites distinguishing tumor tissue from adjacent healthy tissue were common across stages pTa, pT1, and pT2. However, a notable finding emerged in pT1 BC patients, where three metabolites, including C17-sphinganine, palmitamide, and propionylcarnitine, were significantly lower in tumor tissues compared to adjacent healthy tissues. In patients with stage pT2 BC, nine compounds were identified in significantly higher quantities in tumor tissues compared to adjacent healthy ones. These included oleamide, palmitoylcarnitine, PC(16:0/16:0), PC(30:0), PC(35:2), PC(36:3), PC(O-34:1), PC(O-36:5), and stearoylcarnitine, alongside 3-methylhistidine, which was found in significantly lower amounts in tumor tissues compared to healthy adjacent tissues.

5. Conclusion

In summary, our study demonstrates the efficacy of ultra-high-performance liquid chromatography and ultra-high-resolution mass spectrometry in identifying tissue metabolome changes in patients with BC. We have identified thirty-nine metabolites that hold promise for distinguishing cancerous tissue from adjacent normal tissue, considering the differentiation across various grades and stages of BC. Notably, our research represents a novel contribution as there is currently no published evidence highlighting these specific combinations of metabolites as potential crucial markers for early detection of BC. The identified tissue biomarkers of the BC potentially can be used during tumor removal surgery. They might enable surgeons to accurately delineate tumor margins, ensuring the complete removal of cancerous tissue while conserving as much healthy tissue as possible. This precision is particularly crucial in surgeries aimed at preserving organs and in operations near critical structures. This could aid surgeons in distinguishing between cancerous and non-cancerous tissues in real time, a feature that would be especially beneficial in minimally invasive surgeries, such as laparoscopic or robotic procedures, where direct visualization is more challenging. During surgery, they could guide targeted biopsies and intraoperative frozen section analysis, helping to confirm that surgical margins are free of cancer cells. Moreover, we emphasize the importance of considering factors such as stage and grade of malignancy, as they add complexity to the identification of relevant metabolomic signatures in BC.

Ethical approval

The study protocol was approved by the local Bioethics Committee at the University of Rzeszow (Poland) (permission no. 2018/04/10). The patients provided written consent to participate in research. The patients provided written informed consent for the publication of any associated data.

Funding

The research was supported by National Science Centre (Poland), research project SONATA Number UMO-2018/31/D/ST4/00109.

CRediT authorship contribution statement

Ossoliński Tadeusz: Resources. **Krupa Zuzanna:** Writing – original draft. **Ruman Tomasz:** Writing – review & editing, Supervision, Resources, Methodology, Investigation, Data curation. **Nizioł Joanna:** Writing – review & editing, Writing – original draft, Visualization, Supervision, Project administration, Methodology, Investigation, Funding acquisition, Formal analysis, Data curation, Conceptualization. **Ossoliński Krzysztof:** Writing – original draft, Resources, Methodology, Investigation. **Płaza-Altamer Aneta:** Investigation, Data curation. **Kołodziej Artur:** Investigation, Data curation. **Ossolińska Anna:** Resources.

Declaration of generative AI and AI-assisted technologies in the writing process

During the preparation of this work, the author(s) used ChatGPT3 (OpenAI) in order to improve language and readability. After using this tool/service, the author(s) reviewed and edited the content as needed and take(s) full responsibility for the content of the publication.

Declaration of Competing Interest

The authors declare that they have no known competing financial interests or personal relationships that could have appeared to influence the work reported in this paper.

Appendix A. Supporting information

Supplementary data associated with this article can be found in the online version at doi:10.1016/j.jpba.2024.115966.

References

[1] H. Sung, J. Ferlay, R.L. Siegel, M. Laversanne, I. Soerjomataram, A. Jemal, F. Bray, Global cancer statistics 2020: globocan estimates of incidence and mortality worldwide for 36 cancers in 185 countries, CA Cancer J. Clin. 71 (2021) 209–249, https://doi.org/10.3322/CAAC.21660.

[2] M.C.S. Wong, F.D.H. Fung, C. Leung, W.W.L. Cheung, W.B. Goggins, C.F. Ng, The global epidemiology of bladder cancer: a joinpoint regression analysis of its incidence and mortality trends and projection, 8, Sci. Rep. 2018 8 (1) (2018) 1–12, https://doi.org/10.1038/s41598-018-19199-z.

[3] J. Mushtaq, R. Thurairaja, R. Nair, Bladder cancer, Surg. (Oxf.) 37 (2019) 529–537, https://doi.org/10.1016/J.MPSUR.2019.07.003.

[4] D. Sahu, Y. Lotan, B. Wittmann, B. Neri, D.E. Hansel, Metabolomics analysis reveals distinct profiles of nonmuscle-invasive and muscle-invasive bladder cancer, Cancer Med 6 (2017) 2106–2120, https://doi.org/10.1002/CAM4.1109.

[5] S. Tabaei, M.R. Haghshenas, T.J. Webster, A. Ghaderi, Proteomics strategies for urothelial bladder cancer diagnosis, prognosis and treatment: Trends for tumor biomarker sources, Anal. Biochem 666 (2023) 115074, https://doi.org/10.1016/J.AB.2023.115074.

[6] X.W. Zhang, Q.H. Li, Z. Di Xu, J.J. Dou, Mass spectrometry-based metabolomics in health and medical science: a systematic review, RSC Adv. 10 (2020) 3092–3104, https://doi.org/10.1039/C9RA08985C.

[7] N.A. Di Meo, D. Loizzo, S.D. Pandolfo, R. Autorino, M. Ferro, C. Porta, A. Stella, C. Bizzoca, L. Vincenti, F. Crocetto, O.S. Tataru, M. Rutigliano, M. Battaglia, P. Ditonno, G. Lucarelli, Metabolomic approaches for detection and identification of biomarkers and altered pathways in bladder cancer, Int J. Mol. Sci. 23 (2022) 4173, https://doi.org/10.3390/IJMS23084173/S1.

[8] H.A. García-Perdomo, A.M. Dávila-Raigoza, F. Korkes, Metabolomics for the diagnosis of bladder cancer: a systematic review, Asian J. Urol. (2023), https://doi.org/10.1016/J.AJUR.2022.11.005.

[9] P.K. Cheung, M.H. Ma, H.F. Tse, K.F. Yeung, H.F. Tsang, M.K.M. Chu, C.M. Kan, W. C.S. Cho, L.B.W. Ng, L.W.C. Chan, S.C.C. Wong, The applications of metabolomics in the molecular diagnostics of cancer, Expert Rev. Mol. Diagn. 19 (2019) 785–793, https://doi.org/10.1080/14737159.2019.1656530.

[10] N.R. Anwardeen, I. Diboun, Y. Mokrab, A.A. Althani, M.A. Elrayess, Statistical methods and resources for biomarker discovery using metabolomics, 24, BMC Bioinforma. 2023 24 (1) (2023) 1–18, https://doi.org/10.1186/S12859-023-05383-0.

[11] N. Putluri, A. Shojaie, V.T. Vasu, S.K. Vareed, S. Nalluri, V. Putluri, G.S. Thangjam, K. Panzitt, C.T. Tallman, C. Butler, T.R. Sana, S.M. Fischer, G. Sica, D.J. Brat, H. Shi, G.S. Palapattu, Y. Lotan, A.Z. Weizer, M.K. Terris, S.F. Shariat, G. Michailidis, A. Sreekumar, Metabolomic profiling reveals potential markers and bioprocesses altered in bladder cancer progression, Cancer Res 71 (2011) 7376–7386, https://doi.org/10.1158/0008-5472.CAN-11-1154.

[12] P. Tripathi, B.S. Somashekar, M. Ponnusamy, A. Gursky, S. Dailey, P. Kunju, C. T. Lee, A.M. Chinnaiyan, T.M. Rajendiran, A. Ramamoorthy, HR-MAS NMR tissue metabolomic signatures cross-validated by mass spectrometry distinguish bladder cancer from benign disease, J. Proteome Res 12 (2013) 3519–3528, https://doi.org/10.1021/PR4004135/SUPPL_FILE/PR4004135_SI_001.PDF.

[13] D.W.B. Piyarathna, T.M. Rajendiran, V. Putluri, V. Vantaku, T. Soni, F.C. von Rundstedt, S.R. Donepudi, F. Jin, S. Maity, C.R. Ambati, J. Dong, D. Gödde, S. Roth, S. Störkel, S. Degener, G. Michailidis, S.P. Lerner, S. Pennathur, Y. Lotan, C. Coarfa, A. Sreekumar, N. Putluri, Distinct lipidomic landscapes associated with clinical stages of urothelial cancer of the bladder, Eur. Urol. Focus 4 (2018) 907–915, https://doi.org/10.1016/J.EUF.2017.04.005.

[14] K. Ossoliński, T. Ruman, T. Ossoliński, A. Ossolińska, A. Arendowski, A. Kołodziej, A. Płaza-Altamer, J. Nizioł, Monoisotopic silver nanoparticles-based mass spectrometry imaging of human bladder cancer tissue: Biomarker discovery, Adv. Med Sci. 68 (2023) 38–45, https://doi.org/10.1016/J.ADVMS.2022.12.002.

[15] D.W.B. Piyarathna, T.M. Rajendiran, V. Putluri, V. Vantaku, T. Soni, F.C. von Rundstedt, S.R. Donepudi, F. Jin, S. Maity, C.R. Ambati, J. Dong, D. Gödde, S. Roth, S. Störkel, S. Degener, G. Michailidis, S.P. Lerner, S. Pennathur, Y. Lotan, C. Coarfa, A. Sreekumar, N. Putluri, Distinct lipidomic landscapes associated with clinical stages of urothelial cancer of the bladder, Eur. Urol. Focus 4 (2018) 907–915, https://doi.org/10.1016/J.EUF.2017.04.005.

[16] R.R. Bhanvadia, Y. Lotan, Progress in the development of tissue-based biomarkers for urothelial cancer, Expert Rev. Anticancer Ther. 22 (2022) 605–619, https://doi.org/10.1080/14737140.2022.2070154.

[17] H.L. Stewart, D.J.S. Birch, Fluorescence guided surgery, Methods Appl. Fluor. 9 (2021) 042002, https://doi.org/10.1088/2050-6120/AC1DBB.

[18] J. Nizioł, V. Copié, B.P. Tripet, L.B. Nogueira, K.O.P.C. Nogueira, K. Ossoliński, A. Arendowski, T. Ruman, Metabolomic and elemental profiling of human tissue in kidney cancer, Metabolomics 17 (2021) 30, https://doi.org/10.1007/S11306-021-01779-2.

[19] MassBank of North America (MoNA), (n.d.).

[20] Mass Spectrometry Data Center, NIST, (n.d.). ⟨https://chemdata.nist.gov/⟩ (Accessed 8 June 2022).

[21] Z. Pang, J. Chong, G. Zhou, D.A. De Lima Morais, L. Chang, M. Barrette, C. Gauthier, P.É. Jacques, S. Li, J. Xia, MetaboAnalyst 5.0: narrowing the gap between raw spectra and functional insights, Nucleic Acids Res 49 (2021) W388–W396, https://doi.org/10.1093/NAR/GKAB382.

[22] J. Nizioł, K. Ossoliński, A. Płaza-Altamer, A. Kołodziej, A. Ossolińska, T. Ossoliński, A. Nieczaj, T. Ruman, Untargeted urinary metabolomics for bladder cancer biomarker screening with ultrahigh-resolution mass spectrometry, 13, Sci. Rep. 2023 13 (1) (2023) 1–15, https://doi.org/10.1038/s41598-023-36874-y.

[23] K. Ossoliński, T. Ruman, V. Copié, B.P. Tripet, A. Kołodziej, A. Płaza-Altamer, A. Ossolińska, T. Ossoliński, A. Nieczaj, J. Nizioł, Targeted and untargeted urinary metabolic profiling of bladder cancer, J. Pharm. Biomed. Anal. 233 (2023) 115473, https://doi.org/10.1016/J.JPBA.2023.115473.

[24] S. Okuda, T. Yamada, M. Hamajima, M. Itoh, T. Katayama, P. Bork, S. Goto, M. Kanehisa, KEGG Atlas mapping for global analysis of metabolic pathways, Nucleic Acids Res 36 (2008) W423–W426, https://doi.org/10.1093/NAR/GKN282.

[25] J. Nizioł, K. Ossoliński, A. Płaza-Altamer, A. Kołodziej, A. Ossolińska, T. Ossoliński, T. Ruman, Untargeted ultra-high-resolution mass spectrometry metabolomic profiling of blood serum in bladder cancer, 12, Sci. Rep. 2022 12 (1) (2022) 1–13, https://doi.org/10.1038/s41598-022-19576-9.

[26] D.W. Foster, The role of the carnitine system in human metabolism, Ann. N. Y Acad. Sci. 1033 (2004) 1–16, https://doi.org/10.1196/ANNALS.1320.001.

[27] M.V. Liberti, J.W. Locasale, The Warburg effect: how does it benefit cancer cells? Trends Biochem Sci. 41 (2016) 211–218, https://doi.org/10.1016/J.TIBS.2015.12.001.

[28] X. Jin, S.J. Yun, P. Jeong, I.Y. Kim, W.J. Kim, S. Park, Diagnosis of bladder cancer and prediction of survival by urinary metabolomics, Oncotarget 5 (2014) 1635, https://doi.org/10.18632/ONCOTARGET.1744.

[29] B.M. Wittmann, S.M. Stirdivant, M.W. Mitchell, J.E. Wulff, J.E. McDunn, Z. Li, A. Dennis-Barrie, B.P. Neri, M.V. Milburn, Y. Lotan, R.L. Wolfert, Bladder cancer biomarker discovery using global metabolomic profiling of urine, PLoS One 9 (2014) e115870, https://doi.org/10.1371/JOURNAL.PONE.0115870.

[30] J. Nizioł, V. Bonifay, K. Ossoliński, T. Ossoliński, A. Ossolińska, J. Sunner, I. Beech, A. Arendowski, T. Ruman, Metabolomic study of human tissue and urine in clear cell renal carcinoma by LC-HRMS and PLS-DA, Anal. Bioanal. Chem. 410 (2018) 3859–3869, https://doi.org/10.1007/s00216-018-1059-x.

[31] P. Tripathi, P. Kamarajan, B.S. Somashekar, N. MacKinnon, A.M. Chinnaiyan, Y. L. Kapila, T.M. Rajendiran, A. Ramamoorthy, Delineating metabolic signatures of head and neck squamous cell carcinoma: phospholipase A2, a potential therapeutic target, Int J. Biochem Cell Biol. 44 (2012) 1852–1861, https://doi.org/10.1016/J.BIOCEL.2012.06.025.

[32] B.S. Cummings, Phospholipase A2 as targets for anti-cancer drugs, Biochem Pharm. 74 (2007) 949–959, https://doi.org/10.1016/J.BCP.2007.04.021.

[33] S.A. Mir, P. Rajagopalan, A.P. Jain, A.A. Khan, K.K. Datta, S.V. Mohan, S.S. Lateef, N. Sahasrabuddhe, B.L. Somani, T.S. Keshava Prasad, A. Chatterjee, K.V. Veerendra Kumar, M. VijayaKumar, R.V. Kumar, S. Gundimeda, A. Pandey, H. Gowda, LC–MS-based serum metabolomic analysis reveals dysregulation of phosphatidylcholines in esophageal squamous cell carcinoma, J. Proteom. 127 (2015) 96–102, https://doi.org/10.1016/J.JPROT.2015.05.013.

[34] M.Y. Lee, A. Yeon, M. Shahid, E. Cho, V. Sairam, R. Figlin, K.H. Kim, J. Kim, Reprogrammed lipid metabolism in bladder cancer with cisplatin resistance, Oncotarget 9 (2018) 13231, https://doi.org/10.18632/ONCOTARGET.24229.

[35] C. Denkert, J. Budczies, T. Kind, W. Weichert, P. Tablack, J. Sehouli, S. Niesporek, D. Könsgen, M. Dietel, O. Fiehn, Mass spectrometry–based metabolic profiling reveals different metabolite patterns in invasive ovarian carcinomas and ovarian borderline tumors, Cancer Res 66 (2006) 10795–10804, https://doi.org/10.1158/0008-5472.CAN-06-0755.

[36] K.K. Pasikanti, K. Esuvaranathan, Y. Hong, P.C. Ho, R. Mahendran, L. Raman Nee Mani, E. Chiong, E.C.Y. Chan, Urinary metabotyping of bladder cancer using two-dimensional gas chromatography time-of-flight mass spectrometry, J. Proteome Res 12 (2013) 3865–3873, https://doi.org/10.1021/pr4000448.